EPJ Web of Conferences **163**, 00052 (2017) DOI: 10.1051/epjconf/201716300052
FUSION17

First Elastic Scattering Measurement of ^{8}Li on ^{209}Bi at the Australian National University

C. Sengupta[1,⋆], *I.P.* Carter[1], *K.J.* Cook[1], *E.C.* Simpson[1], *M.* Dasgupta[1], *D. J.* Hinde[1], *D.Y.* Jeung[1], *Sunil* Kalkal[1,2], *K.* Vo-Phuoc[1], *E.* Prasad[1], *D.* Rafferty[1], *C.* Simenel[1], and *E.* Williams[1]

[1] *Department of Nuclear Physics, Research School of Physical Sciences and Engineering, The Australian National University, Canberra, ACT 0200, Australia*
[2] *Thapar University, Patiala, India*

Abstract. The effects of unusual structures of nuclei, such as neutron halos, on nuclear reaction mechanisms are not well understood, particularly at near barrier energies. Using the SOLEROO Radioactive Ion Beam facility at the Australian National University, below-barrier reactions with ^{8}Li incident on ^{209}Bi have been performed. Beam purities of about 95% are achieved by rejecting unwanted beam species using a solenoidal separator along with tracking and tagging the secondary beam with two parallel plate avalanche counters (PPACs) placed immediately after the solenoid. However, the radioactive ion beam exiting the solenoid is not parallel to the primary beam axis. To obtain a precise angular distribution of elastic scattering, the tracking facility is used to deduce the true scattering angle on an event-by-event basis. The elastic cross-section for ^{8}Li on ^{209}Bi is then extracted, verifying the capability of the facility to perform precise cross-section measurements.

1 Introduction

A suppression of complete fusion at above barrier energies has been observed in reactions with light, weakly bound nuclei. A series of fusion cross-section measurements performed for ^{9}Be bombarding on ^{208}Pb and ^{209}Bi [1–4], ^{6,7}Li on ^{209}Bi [2, 3, 5] and ^{9,10,11}Be on ^{209}Bi [6] indicate that the complete fusion cross-sections at energies around and above the barrier are suppressed by 30%, compared with reactions of nuclei having a high energy threshold against breakup [2]. Many measurements have also been performed to understand the role of breakup in suppression of fusion cross-sections [7, 8]. However, the impact of breakup on fusion with weakly bound radioactive nuclides is not yet clear.

In exotic nuclei such as ^{8}Li or ^{6}He, containing weakly bound neutrons around a relatively tightly bound core, the nucleon density distribution has an extensive tail which may help the attractive nuclear forces begin to act at large distances between the projectile and the target. This may lower the barrier and enhance fusion cross-sections, particularly in the sub-barrier energy region [9, 10]. However, these nuclei are weakly bound and it is quite possible that their interaction with the target may cause them to breakup. In turn, this may prevent or hinder complete fusion of the projectile with the target [11, 12].

To achieve a better understanding about these exotic nuclei, the SOLEROO Radioactive Ion Beam (RIB) facility has been developed at the Australian National University [13]. Here, we first briefly describe SOLEROO RIB facility. This has been used to study ^{8}Li elastic scattering from ^{209}Bi as a first step towards measuring reaction cross-section of the above system. To extract a reliable angular distribution, the trajectories of the ^{8}Li ions onto the secondary target have been reconstructed. From the reconstructed quantities, the true scattering angle of the scattered ^{8}Li has been obtained for each incident event. The importance of obtaining the true scattering angle is then discussed.

2 The Radioactive Ion Beam Facility at ANU

The SOLEROO RIB facility at the Australian National University is based on a super-conducting solenoidal separator [14–17] which produces RIBs by in-flight transfer reactions via interactions with a primary target. The primary

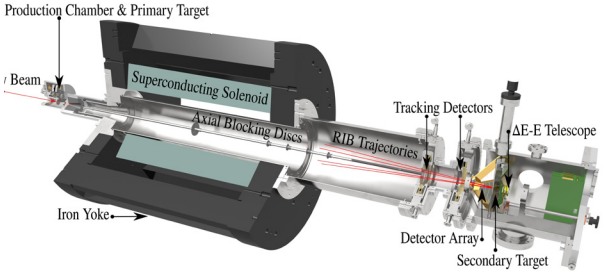

Figure 1. RIB trajectories from the primary target chamber on to the secondary target [18].

⋆e-mail: Chandrima.Sengupta@anu.edu.au

beam of ^{7}Li was provided by the 14UD tandem accelerator and bombarded a 5.572 mg/cm^2 ^{9}Be primary target, producing a secondary beam of ^{8}Li. This neutron pickup reaction has a positive Q value of 368 keV. Following production, the transfer products enter a magnetic field region (2° - 6° acceptance) and the desired RIBs are separated using a 6.5 T axial magnetic field [14] and focussed on to a secondary target [18]. The direct beam is stopped by a Faraday cup. The unwanted beam species are focussed on to an axial rod or stopped by axial blocking discs depending on their focal lengths.

After the solenoid, there are two position sensitive parallel plate avalanche counters (PPACs) [16, 17]. These detectors are used to track the RIB on its path to the secondary target. Fig. 1 shows a schematic of the device and the beam trajectories originating from the primary target chamber passing through the solenoid, focussed on to the secondary target. The reaction products produced from the secondary target are detected by a large area position sensitive detector array (BALiN) [19].

2.1 Tracking System

Using a single solenoid, a maximum purity of 30% can be achieved in this reaction [13, 18]. The PPACs placed at the exit of the solenoid help to reject the unwanted beam species and a purity greater then 95% can be achieved for ^{6}He and ^{8}Li beam [17] by tagging and tracking the beam species. The PPACs [20] consist of two X-Y position foils and one centre foil. The X-Y position foils are negatively biased aluminised Mylar (50 nm aluminium on 0.9 μm Mylar foil), having x, y position strips spaced by 1 mm, allowing us to achieve position sensitivity of less than 1mm [17]. The signal in the position foils is passed through delay lines and is collected as a difference of time taken by the signal to travel to the two ends of the delay line. The X-Y position information collected from the two PPACs allows tracking of the secondary beam on its path to the secondary target. The centre foil of 0.9 μm Mylar is positively biased and coated with 50 nm Aluminium on both sides. The spacing between each foil is 4 mm and the PPAC has a square active area of 35 × 35 mm^2. The total applied bias was kept constant at 880 V across the detector, where -250 V was applied on the X, Y signal foils and +630 V on the centre foil. The filling gas (Propane) is circulated at 10 Torr between the foils using a gas flow system [18]. The detector window was made up of 0.9 μm Mylar. When charged particles pass through the detector, electron-ion pairs are generated, which are collected by the anodes and cathodes, respectively. Electrons, being lighter than the ions, produce the fastest signal and therefore this signal is used to generate timing information. This allows us to electronically identify and tag the beam species using the energy loss in the centre foil and Time of Flight (ToF) information [18].

2.2 Experimental Setup

The scattered ^{8}Li particles from ^{209}Bi were measured using the Breakup Array for Light Nuclei (BALiN). This array consists of four double sided Silicon strip detectors.

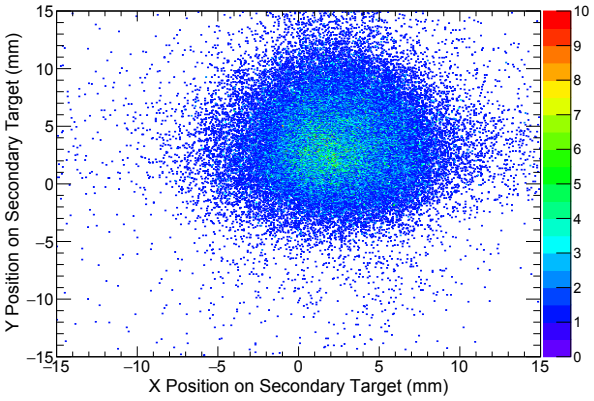

Figure 2. Reconstructed beam profile on the secondary target.

Each detector is 400 μm thick, with 16 arcs and 8 sectors, giving a total of 512 position pixels. It has a total effective area of 80 cm^2, having inner radius of 32.6 mm and outer radius of 135.1 mm. Each sector covers 6.8° in azimuthal angle ϕ. A 0.7 μm Mylar foil was placed in front of the front detectors to stop electrons. One of the detectors in the backward angles was not useful for elastic scattering as the gain of the preamplifier was set too high. The two forward detectors covered 20° to 90° in scattering angle θ and 16° to 164° in ϕ and the backward detector covered 90° to 162° in θ and 273° to 345° in ϕ.

3 Reconstruction of Beam Profile on the Secondary Target

The energy of the RIB produced in the primary target will vary depending on its exit angle from the primary target, the interaction point on the primary target and the excited state in which ^{8}Li is produced. As the acceptance of the solenoid is between 2° and 6° in the laboratory frame, the RIB exits the solenoid at angles between 2° and 6°, and will have a finite beam spot size on the secondary target. Therefore, it is necessary to know the exact interaction point of the beam on the secondary target. Using the two position sensitive tracking detectors, it is possible to define a direction vector of the RIB and extrapolate it to the secondary target plane to reconstruct the beam profile on the secondary target. This calculation is done on an event-by-event basis. Fig. 2 shows the reconstructed beam profile of the elastically scattered events of ^{8}Li on the secondary target ^{209}Bi. The FWHM of the beam profile on the secondary target is around 8 mm. The offset of the beam in y arises due to the misalignment of the solenoid axis with the primary beam axis while the offset in x comes due to the steering elements along the beam line.

4 Reconstruction of focal length of the Secondary Beam

The RIB of ^{8}Li is produced in the primary target chamber in the interaction of ^{7}Li with the ^{9}Be primary target. Along with the desired beam species, some other contaminant ions such as $^{1}_{1}$H^{+}, $^{2}_{1}$H^{+}, $^{3}_{1}$H^{+}, $^{4}_{2}$He^{2+}, $^{6}_{3}$Li^{3+}, $^{7}_{3}$Li^{3+} have

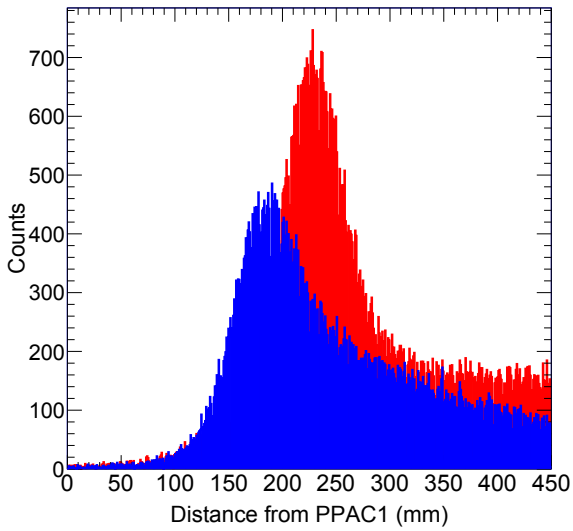

Figure 3. Reconstructed focal point of the elastically scattered ^{8}Li ground state (red) and first excited state (blue) from PPAC1.

also been identified [18]. $^{1}_{1}H^{+}$, $^{2}_{1}H^{+}$, $^{3}_{1}H^{+}$ and $^{4}_{2}He^{2+}$ produced from ^{7}Li breakup [18] generates a broad energy distribution. As a result, other particles along with ^{8}Li can pass through the solenoid and hit the secondary target.

To separate these unwanted species, a software routine has been developed to calculate the focal point on an event-by-event basis. Applying a cut on the focal length allows selection of desired species of a particular energy. Fig. 3 shows the reconstructed focal point of the elastically scattered ^{8}Li particles (red denotes the ground state and the blue denotes the first excited state of ^{8}Li) on the primary beam axis assuming the origin at PPAC1.

The most problematic species which is transmitted to the secondary target is energy degraded ^{7}Li [18]. If the ^{7}Li primary beam scatters off some surface and then has the same rigidity as ^{8}Li, it will be transported to the secondary target. By carefully adjusting the primary beam tune, the contamination of $^{7}_{3}Li^{3+}$ can be minimised.

5 Reconstruction of True Scattering Angle

The RIB exiting the solenoid and incident on the secondary target is not parallel to the primary beam axis and makes an angle, θ_{Beam}, with the primary beam axis. The geometric angle of a detector pixel, θ_{Geom} is the angle associated with a vector constructed between the centre of the secondary target and the pixel hit on BALiN, with respect to the primary beam axis. The true scattering angle (θ_{RIB}) will depend on the interaction point of the ^{8}Li projectile on the secondary target and θ_{Beam} for that projectile, and thus can be significantly different from θ_{Geom}. Here, θ_{Geom}, θ_{RIB} and θ_{Beam} are in the laboratory frame.

To derive a relationship between θ_{Geom} and θ_{RIB}, an intermediate angle, $\theta_{\mathrm{Parallel}}$ is reconstructed using a routine in the software, where $\theta_{\mathrm{Parallel}}$ is the scattering angle of any event if the incident RIB is parallel to the primary beam axis. Essentially, $\theta_{\mathrm{Parallel}}$ takes into account the interaction point of the RIB particle on the secondary target.

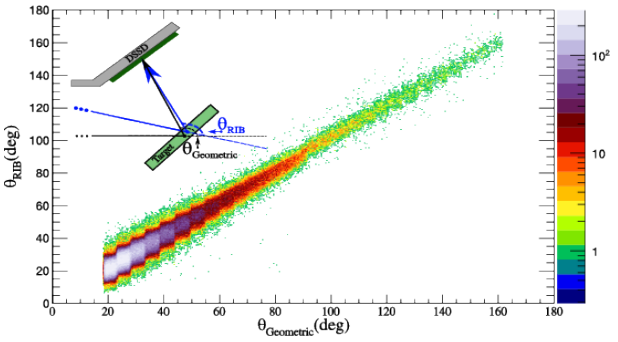

Figure 4. Conversion between θ_{Geom} and θ_{RIB} for the system ^{8}Li on ^{209}Bi at E_{lab}=26.88 MeV [18].

The relationship derived from simple geometry is shown below for conversion between $\theta_{\mathrm{Parallel}}$ and θ_{RIB}:

$$\cos(\theta_{\mathrm{RIB}}) = \cos(\theta_{\mathrm{Beam}})\cos(\theta_{\mathrm{Parallel}}) - \sin(\theta_{\mathrm{Parallel}})\sin(\theta_{\mathrm{Beam}})\cos(\phi_{\mathrm{Beam}} - \phi_{\mathrm{Parallel}}) \quad (1)$$

Therefore, to reconstruct the true scattering angle we need to know the angle of incidence of the beam (θ_{Beam}) on the secondary target, and the exact interaction point of the beam on the secondary target. These can be found using the tracking system, as discussed previously.

The distribution of events with θ_{RIB} and θ_{Geom} from the experimental data of ^{8}Li on ^{209}Bi at E_{lab}=26.88 MeV is shown in the Fig. 4. It can be seen that for a particular θ_{Geom}, there is a spread in θ_{RIB}. The full width half maximum of the Gaussian distribution of θ_{RIB} corresponding to a given θ_{Geom} is around 7° over the full angular range covered by the detectors. As mentioned earlier in Sec. 2, the acceptance of the solenoid is between 2° and 6°. Therefore, much of the spread in θ_{RIB} comes from this factor. Also there is a finite beam spot size on the secondary target mentioned above and pixelization of the BALiN array, will introduce some spread in θ_{RIB}.

6 Preliminary result of elastic scattering of ^{8}Li by ^{209}Bi

Elastic scattering measurements of ^{8}Li on ^{209}Bi were carried out using the 14UD accelerator at the Australian National University. The primary beam of ^{7}Li was accelerated at an energy of 32 MeV, ^{8}Li was produced in a transfer reaction of ^{7}Li on ^{9}Be. The solenoid field was set to 3.11 T to optimally transport ^{8}Li ions. The ^{209}Bi target, rotated to 45°, had a thickness of 1.22 mg/cm^{2}. Taking the energy loss in the primary target and in the PPACs into account, the secondary beam energy in the laboratory frame incident on the secondary target is 26.88 MeV. At this below-barrier energy, we would expect the majority of the elastic scattering to be purely Rutherford scattering. One of the forward arcs at 58.5° where there is no edge effect, has been used as the monitor to normalize the elastic cross-section.

To extract elastic cross-sections for the above system, a software gate was applied to select the elastically scattered events of ^{8}Li in its ground state and 0.98 MeV first

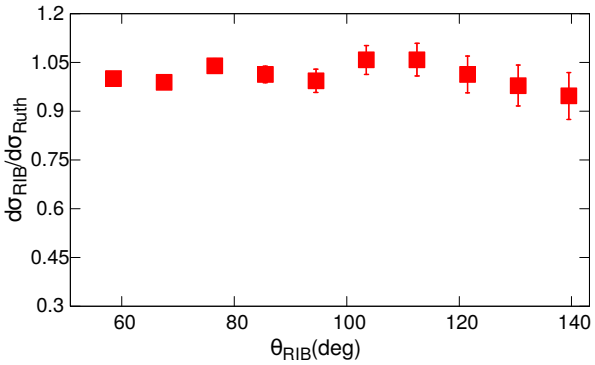

Figure 5. Ratio of elastic scattering cross-section to Rutherford cross-section as a function of θ_{RIB} for the system ^{8}Li on ^{209}Bi at E_{lab}=26.88 MeV.

excited state. At the final stage of data processing, the experimental data is binned in 9° steps in θ_{Geom} and θ_{RIB}.

The next step is to find the yield for each θ_{RIB} bin. In order to calculate the solid angle of each θ_{Geom} bin, we simulate the events over 4π sr, and filter through the known detector geometry. The coordinate system of BALiN pixels is defined with respect to the centre of the secondary target and the geometric solid angle ($d\Omega_{\mathrm{Geom}}$) is therefore calculated as a function of θ_{Geom} in the simulation. Within the data binned as a function of θ_{Geom} and θ_{RIB}, a bin by bin efficiency correction is made, and then projected on to the θ_{RIB} axis to extract the true angular distribution. Then to extract the elastic cross-section as a function of θ_{RIB}, we use the following equation:

$$\frac{d\sigma}{d\Omega_{\mathrm{lab}}} = \frac{Y(\theta_{\mathrm{det}}, E)}{Y(\theta_{\mathrm{Monitor}}, E)} \frac{d\sigma}{d\Omega_{\mathrm{Monitor}}} \qquad (2)$$

Where, $\frac{d\sigma}{d\Omega_{\mathrm{lab}}}$ is the elastic cross-section determined as a function of θ_{RIB}, Y(θ_{det},E) is the yield in each θ_{RIB} bin, Y($\theta_{\mathrm{Monitor}}$,E) is the yield in the monitor bin and $\frac{d\sigma}{d\Omega_{\mathrm{Monitor}}}$ is the elastic cross-section of that monitor bin.

Fig. 5 shows the ratio of elastic cross-section to Rutherford cross-section of ^{8}Li on ^{209}Bi at 26.88 MeV as a function θ_{RIB}. We only show the data that falls within the geometric coverage of the detector having no edge effect. The statistical uncertainty in cross-section is smaller than the points at the forward angles but bigger at the backward angles. This result looks reasonable, but will be refined in future work as described below.

7 Conclusion and Future Work

This paper has discussed elastic scattering of ^{8}Li on ^{209}Bi measured using the SOLEROO RIB facility at the Australian National University. A transformation relation between θ_{RIB} and θ_{Geom} has been established to calculate the true scattering angle. Using this relationship, θ_{RIB} has been reconstructed event-by-event in the experimental data. Then the yield for each θ_{RIB} bin is corrected for efficiency. Then the elastic cross-section is obtained as a function of θ_{RIB}.

The above correction implemented in the simulation is a first order correction. In future, the beam interaction point on the secondary target will be taken into account to calculate the geometric efficiency.

The effect of the misalignment of the solenoid with the primary beam axis is expected to have small effect on reconstruction of the true scattering angle. However, work is under process to test the effect of this misalingnment on the reconstructed quantities.

Implementing this correction in the data analysis, an optical model fit would allow us to get the optical potential parameters using FRESCO [21] and extract the reaction cross-section.

References

[1] M. Dasgupta, D. J. Hinde, R. D. Butt, R. R. M. Anjos, A. Berriman, N. Carlin, P. R. S. Gomes, C. C. R. Morton, J. O. J. Newton, A. Szanto de Toledo, Others, and K. Hagino, Phys. Review Letters, Journal **82**, 1395 (1999).

[2] M. Dasgupta, P. R. S. Gomes, D. J. Hinde, S. Moraes, R. Anjos, A. Berriman, R. Butt, N. Carlin, J. Lubian, C. Morton, and Others, Phys. Review C, Journal **70**, 024606 (2004).

[3] C. Signorini, T. Glodariu, Z. H. Liu, M. Mazzocco, M. Ruan, and F. Soramel, Progress of Theoretical Physics Supplement, Journal **154**, 272 (2004).

[4] M. Dasgupta, D. J. Hinde, S. L. Sheehy, and B. Bouriquet, Phys. Review C, Journal **81**, 024608 (2010).

[5] M. Dasgupta, D. J. Hinde, K. Hagino, S. Moraes, P. R. S. Gomes, R. Anjos, R. Butt, A. Berriman, N. Carlin, C. Morton, J. Newton, and A. Szanto de Toledo, Phys. Review C, Journal **66**, 041602(R) (2002).

[6] D. J. Hinde and M. Dasgupta, Phys. Review C, Journal **81**, 064611 (2010).

[7] K. J. Cook, E. C. Simpson, D. H. Luong, Sunil Kalkal, M. Dasgupta, and D. J. Hinde, Phys. Review C, Journal **93**, no. 6, 1-15 (2016).

[8] Sunil Kalkal, E. C. Simpson, D. H. Luong, K. J. Cook, M. Dasgupta, D. J. Hinde, I. P. Carter, D. Y. Jeung, G. Mohanto, C. S. Palshetkar, E. Prasad, D. C. Rafferty, C. Simenel, K. Vo-Phuoc, and E. Williams, Phys. Review C, Journal **93**, 1-13 (2016).

[9] J. J. Kolata et al., Phys. Review C, Journal **65**, 054616 (2002).

[10] A. M. Moro et al., Phys. Review C, Journal **68**, 034614 (2003).

[11] E. F. Aguilera et al., Revista mexicana de física, Journal **50**, 1–4 (2004).

[12] E. F. Aguilera et al., Phys. Review C, Journal **80**, 044605 (2009).

[13] A. J. Horsley, D. J. Hinde, M. Dasgupta, R. Rafiei, A. Wakhle, M. Evers, D. H. Luong, R. du Rietz, Nucl. Instr. Meth. In Phys. Res. A, Journal **646**, 174 (2011).

[14] R. Rafiei, D. J. Hinde, M. Dasgupta, D. C. Weisser, A. G. Muirhead, A. B. Harding, A. K. Cooper, H. J. Wallace, N. R. Lobanov, A. Wakhle, M. L. Brown, C. J. Lin, A. J. Horsley, R. du Rietz, D. H. Luong, and M. Evers, Nucl. Instruments Methods Phys. Res.

Sect. A Accel. Spectrometers, Journal **631**, 12–21 (2011).

[15] H. Laurent and J. Schapira, Nuclear Instruments and Methods, Journal **162**, 181 – 192 (1979).

[16] I. P. Carter et al., EPJ Web of Conferences,Journal **63**, 02022 (2013).

[17] I. P. Carter et al., EPJ Web of Conferences, Journal **91**, 00001 (2015).

[18] I. P. Carter, *Developing Techniques For High Fidelity Studies of Reactions With Light Weakly Bound Nuclei* (Ian Paul Carter, The Australian National University, 2016).

[19] K. J. Cook, *Zeptosecond dynamics of transfer-triggered breakup: mechanisms, timescales, and consequences for fusion* (Kaitlin Jennifer Cook, The Australian National University, 2016) 82-87.

[20] Glenn F. Knoll, *Radiation Detection and Measurement* (John Wiley & Sons, United States of America, 1999) 160.

[21] I. J. Thompson, Comput. Phys. Rep., Journal **7**, 167 (1988).